THE JOURNAL OF PHYSICAL CHEMISTRY C

Article

pubs.acs.org/JPCC

Multilayer Two-Dimensional Water Structure Confined in MoS_2

Kijeong Kwac,[†] In Kim,[†] Tod A. Pascal,[⊥] William A. Goddard,[§] Hyung Gyu Park,[†,‡] and Yousung Jung*[,†]

[†]Graduate School of Energy, Environment, Water, and Sustainability (EEWS) and KAIST Institute NanoCentury, Korea Advanced Institute of Science and Technology (KAIST), 291 Daehakro, Yuseong-gu, Daejeon 34141, Republic of Korea

[⊥]The Molecular Foundry, Lawrence Berkeley National Laboratory, Berkeley, California 94720, United States

[§]Materials and Simulations Process Center, Division of Chemistry and Chemical Engineering, California Institute of Technology, Pasadena 91125, United States

[‡]Nanoscience for Energy Technology and Sustainability, Department of Mechanical and Process Engineering, Eidgenössische Technische Hochschule (ETH) Zürich, Tannenstrasse 3, Zürich 8092, Switzerland

Supporting Information

ABSTRACT: The conflicting interpretations (square vs rhomboidal) of the recent experimental visualization of the two-dimensional (2D) water confined in between two graphene sheets by transmission electron microscopy measurements, make it important to clarify how the structure of two-dimensional water depends on the constraining medium. Toward this end, we report here molecular dynamics (MD) simulations to characterize the structure of water confined in between two MoS_2 sheets. Unlike graphene, water spontaneously fills the region sandwiched by two MoS_2 sheets in ambient conditions to form planar multilayered water structures with up to four layer. These 2D water molecules form a specific pattern in which the square ring structure is formed by four diamonds via H-bonds, while each diamond shares a corner in a perpendicular manner, yielding an intriguing isogonal tiling structure. Comparison of the water structure confined in graphene (flat uncharged surface) vs MoS_2 (ratchet-profiled charged surface) demonstrates that the polarity (charges) of the surface can tailor the density of confined water, which in turn can directly determine the planar ordering of the multilayered water molecules in graphene or MoS_2. On the other hand, the intrinsic surface profile (flat vs ratchet-profiled) plays a minor role in determining the 2D water configuration.

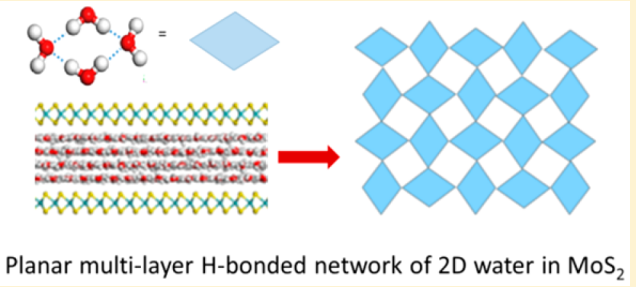

INTRODUCTION

When water is confined inside a narrow nanoscale tube or between solid walls separated by a distance commensurable with the molecule's own dimension, their structural and dynamical properties can change drastically from those of bulk water.[1−11] Inside a one-dimensional channel of carbon nanotubes, for example, water molecules could undergo unconventional phase transitions[12,13] and form ice-like structures at room temperatures depending on the channel diameter. Also, a delicate balance between entropy and enthalpy can render these confined water thermodynamically more stable than the bulk water.[3,14,15] Theoretical investigations of the structures of the two-dimensional (2D) water confined in between the flat walls have suggested puckered rhombic monolayer ice, planar hexagonal, or amorphous phases depending on the conditions and models employed in the simulations.[16−29]

Although the structures of confined water have been predicted for a variety of dimensions and materials using molecular dynamics (MD) simulations, the first experimental observation of the 2D water in between the two graphene sheets was obtained very recently using high-resolution transmission electron microscopy measurements (TEM).[30] This observation revealed the formation of a monolayer of planar "square" ice with a high packing density and, depending on the intergraphene distance, the formation of bi- and trilayer crystallites of water.[30] The same authors have also reported the MD simulations of graphene-confined water that agreed with the experimental structure of the "square ice". However, this involved an enormous lateral van der Waals pressure of about 1 GPa (10 000 atm) to obtain a flat structure of water for the bilayer and trilayer distances. Indeed the latter measurements and interpretations have been challenged by Zhouet al.,[31] posing the possibility that the square ice structure obtained by Algara-Siller et al.[30] might have been due to a salt contaminant, and that, otherwise, the structures of the graphene-sandwiched water might be slightly rhomboidal without a square symmetry. Therefore, further investigations, both experimental and theoretical, are needed to clarify the structure of the 2D water and the existence of "square" or "rhomboidal" ice.

Received: May 27, 2017
Revised: July 4, 2017
Published: July 5, 2017

DOI: 10.1021/acs.jpcc.7b05153
J. Phys. Chem. C 2017, 121, 16021−16028

In this work, we use molecular dynamics (MD) simulations to predict the structure and energetics of water confined in between two sheets of MoS_2, a 2D material with a ratchet-like nonplanar surface profile. We find that the structure of water confined between the MoS_2 layers exhibits a well-ordered configuration consisting of both of square and rhomboidal local moieties forming an interesting isogonal tiling configuration. A key difference between the graphene and the MoS_2 cases is that the MoS_2 confinement holds clearly separated single, double, triple, and quadruple layers of water depending on the gap spacing of MoS_2 sheets at ambient conditions *without a large lateral pressure*, unlike graphene. Analyzing the similarities and disparities of the graphene vs MoS_2 confined water structures offer insights into the factors that control the structure of 2D water in general.

METHODS

The simulation system consists of two MoS_2 layers and reservoirs of water as shown in Figure 1. The graphene sheets

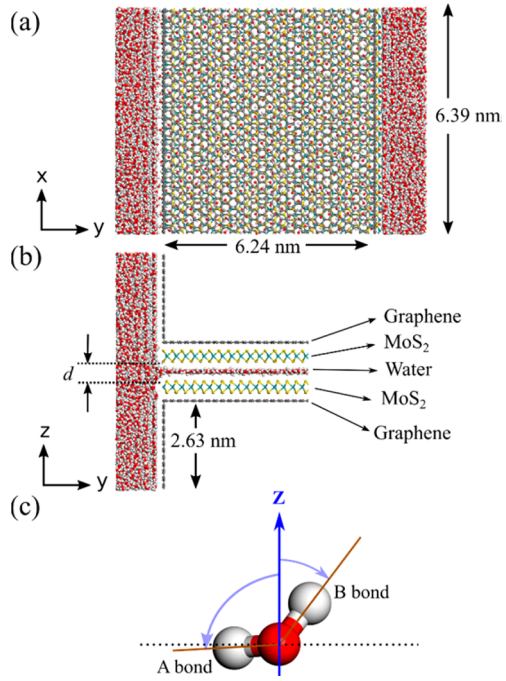

Figure 1. (a, b) System setup for the MD simulation. Oxygen atom is in red, hydrogen in white, Mo in green, S in dark yellow, and carbon in gray. (c) Definition of the A and B bonds of a water molecule used in analysis. Of the two OH bonds of a water molecule, the one nearer to the *xy*-plane is defined as the A bond and the other is the B bond.

are used as a support for MoS_2 and make a channel configuration for simulation purposes. The area of simulated MoS_2 layer is 64.78 × 63.86 Å. For all MD simulations, we fixed the atomic positions of the graphene and MoS_2 layers. We define the interlayer distance, d, of MoS_2 as the difference in z-coordinate between the nearest S atoms of the two MoS_2 layers. The z-dimension of the simulation box depends on the value of the MoS_2 interlayer distance d. The total number of water molecules is varied from 6438 for d = 5.5 Å to 7263 for d = 13 Å, depending on the MoS_2 interlayer distance.

We used the extended simple point charge (SPC/E) model[32] to describe the water molecules. For the van der Waals interaction between water and graphene, we used the parameters from Pascal et al.[14] For the van der Waals interaction between water and MoS_2, we fitted the Lennard-Jones parameters to the potential energy curves obtained by DFT calculations (PBE functional[33] and D2 van der Waals correction[34]) on a model system having a single water molecule in three different configurations on a layer of MoS_2; water molecule on the S atom, Mo atom, and the center position of the hexagon formed by Mo and S atoms (see Figure S1 and S2). For the Lennard-Jones interaction between the other pairs of different types of atoms, we applied the Lorentz−Berthelot rules. The force field parameters are summarized in Tables S1 and S2 of the Supporting Information.

The inner and outer cutoff distance of the Lennard-Jones potential was 10 and 12 Å, respectively, so that the energy and force smoothly changed to zero between the inner and outer cutoffs. The cutoff for the direct Coulomb interaction used was 12 Å and the long-range Coulomb interaction was computed by the particle−particle particle-mesh method.[35] We used the LAMMPS program package[36] for all MD simulations of this work. In the initial setup, water molecules were in the reservoir region with the space between the MoS_2 layers empty. We implemented 500 steps of steepest descent and 1000 steps of conjugate gradient minimization followed by 200 ps equilibration in *NVT* ensemble and subsequent 1 ns equilibration with constant Np_yT condition where only the y-dimension of the simulation box was adjusted at 298 K and 1.0 atm. Then we performed 8 ns production run with the same Np_yT condition, in which the last 4 ns of the production trajectories were used for analysis. The time step used was 1 fs.

Two water molecules were considered to be hydrogen-bonded when oxygen−oxygen distance is less than 3.5 Å and the angle between the O···O axis and the involved OH bond is less than 30°.[37] In the production run we saved snapshots at every 2 ps except for the calculation of the H-bond correlation function for which we performed a separate simulation for 6.0 Å gap spacing to save snapshots at every 0.2 ps.

We define the binding energy of a water molecule as the sum of the electrostatic and van der Waals interaction between the selected water molecule and all the other water molecules and MoS_2 in the simulation box. In the calculation of the binding energy, cutoff distance is not imposed, but instead, pairwise interaction of all the atoms in the simulation box was considered with a minimum image convention.

For comparison, we also performed MD simulations of water between graphene sheets in an infinite graphene configuration, fixing the density of confined water to be the same as in MoS_2. The number of water molecules thus used was 567, 1091, 1646, and 2142 for d = 6, 8, 11, and 13 Å, respectively. The simulation box dimension used was 63.95 × 63.90 × 99.0 Å with the graphene sheets on the xy plane. For water between infinite graphene sheets, the system was equilibrated for 20 ns in the *NVT* ensemble with 298 K followed by 4 ns production run with the same *NVT* condition.

The simulation setup for MoS_2 has the graphene sheets located on the MoS_2. The presence of graphene on MoS_2 cannot have any significant effects on the dynamics of water because the distance from graphene to the O atom of nearest water molecules is about 8.5 Å, a distance that is large enough to make the Lennard-Jones interaction energy between this fictitious graphene and water as small as -0.007ϵ where $-\epsilon$ is the energy minimum of the LJ potential. In addition, graphene has zero charge to have any electrostatic interaction with water.

DOI: 10.1021/acs.jpcc.7b05153
J. Phys. Chem. C 2017, 121, 16021−16028

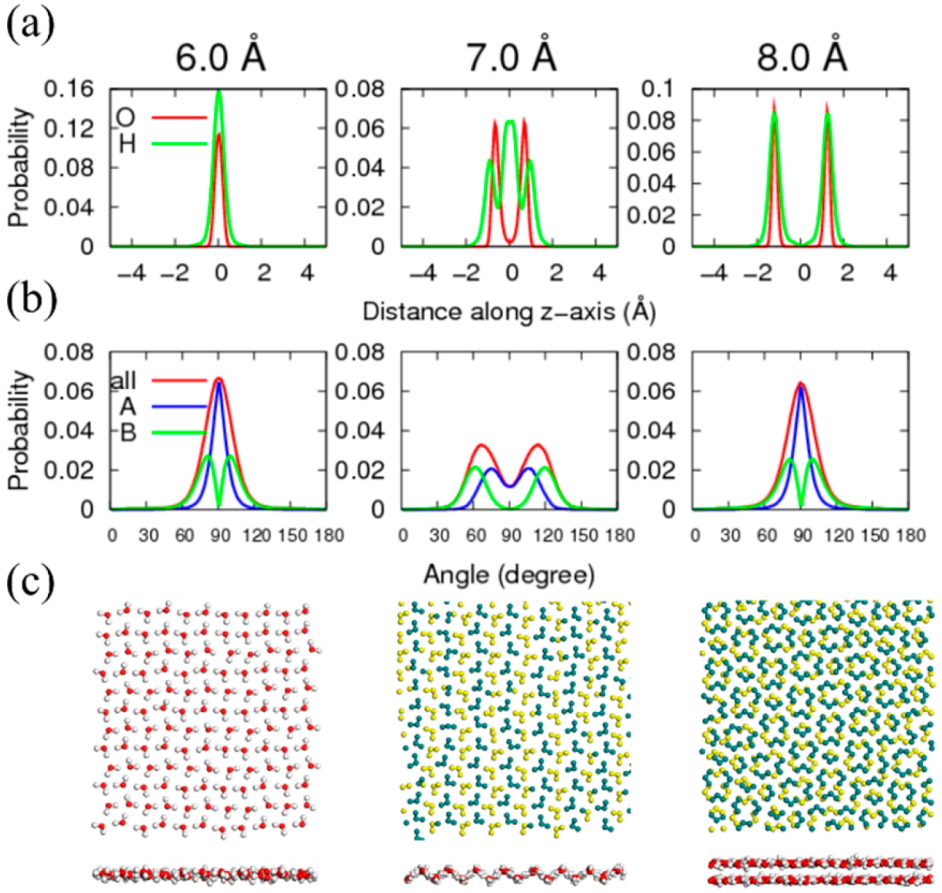

Figure 2. (a) Density profile of O and H atoms of water molecules between MoS_2 sheets separated by a distance d, for d = 6, 7, and 8 Å. Here z = 0 corresponds to the z-center of the gap spacing. (b) Probability density distribution of the angle between the A or B bond (see Figure 1c) and the z-axis. (c) Top and side view of the configuration of water molecules between MoS_2 sheets taken from the MD simulation trajectories. For the top view different colors are used for the atoms below and above the z-center of the gap spacing. Similar density profiles and angle distributions for all other interlayer spacings from 6 to 13 Å in an interval of 0.5 Å are shown in Figures S3–S6.

RESULTS AND DISCUSSION

Water molecules are found experimentally[38] to fill in the confined space between MoS_2 layers spontaneously at ambient conditions. In the current simulations also, after the start of Np_yT equilibration at 298 K and 1 atm, the confined region between the two MoS_2 sheets becomes completely filled with water molecules in less than 200 ps if the S-to-S interlayer distance of the sandwiched MoS_2 sheets (denoted as d) is equal to or larger than 6.0 Å. When the gap is 5.6 Å, it takes about 4 ns for water to fill the confined space. Structures of the confined water are analyzed in detail below using the second half of the subsequent 8 ns-long trajectories under Np_yT conditions at 298 K and 1 atm.

Density profiles of O and H atoms of the 2D water (Figure 2 and Figures S3 and S4) clearly show the single, double, triple, and quadruple layers of water for d = 6, 8, 11, and 13 Å, respectively, where most hydrogen (H−) bonds between water molecules form within the water layer. In contrast, we observe interlayer H-bonds only rarely (1.2, 1.8, and 2.7% for d = 8, 11, and 13 Å). Beyond d = 13 Å, we do not observe a well-defined layered structure due to a high population of the interlayer H-bonds. For intermediate spacing such as d = 7 and 10 Å, high populations of interlayer (or out-of-plane) H-bonds are observed. The fact that the majority of H-bonds for d = 6, 8, 11, and 13 Å remain as the intralayer bonding is consistent with the analysis of water configurations in terms of planarity, as summarized in Figures S5, S6, and S14A.

Interestingly, the density profiles of water for d = 6 and 8 Å are similar to those observed in graphene confined water,[30] suggesting similar H-bond configurations of water regardless of material difference. However, the key disparity is that, for a given interlayer distance of MoS_2 sheets, clearly separated single, double, triple, and quadruple layers are seen at ambient conditions; whereas for graphene, a large lateral pressure is needed not just to bring water to the graphitic confinement but also to obtain a flat configuration. We discuss the origin of this difference later.

A typical MD snapshot is shown in Figure 3B. We see a diamond-shaped local configuration shared by four water molecules via H-bonds, suggesting a particular pattern of the 2D water, or a distorted square isogonal tiling that these diamond units form; the square ring structure is formed by four diamonds via H-bonds, with each pair of diamond sharing a vertex in a perpendicular manner. We denote this configuration by perpendicularly crossing diamonds (*pcd*) in this work. At d = 6 Å, on average 85% of the molecules in the water layer between MoS_2 sheets assume this configuration.

Next, we estimate the energetic gain obtained by the formation of the ordered *pcd* array. In Figure 4A, we show the number of water molecules entering the confined 2D region as a function of time during the equilibration. Water molecules

DOI: 10.1021/acs.jpcc.7b05153
J. Phys. Chem. C 2017, 121, 16021−16028

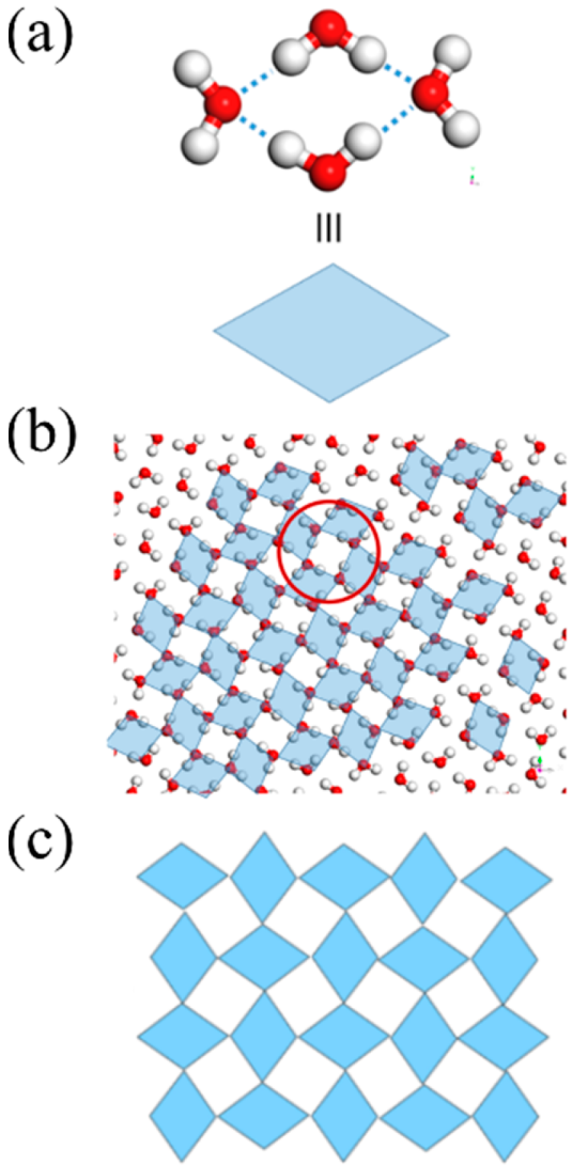

Figure 3. (a) Configuration of four water molecules taken from a MD snapshot in which oxygen atoms form a shape of a diamond. (b) Configuration of confined water molecules taken from the MD simulation for the case of 6.0 Å spacing with superimposed diamond shapes. The red circle points the square configuration of oxygen atoms of the ring of four water molecules. (c) Schematic of the isogonal-tiling planar configuration of 2D water in which the diamond shapes are arranged in a perpendicularly crossing manner.

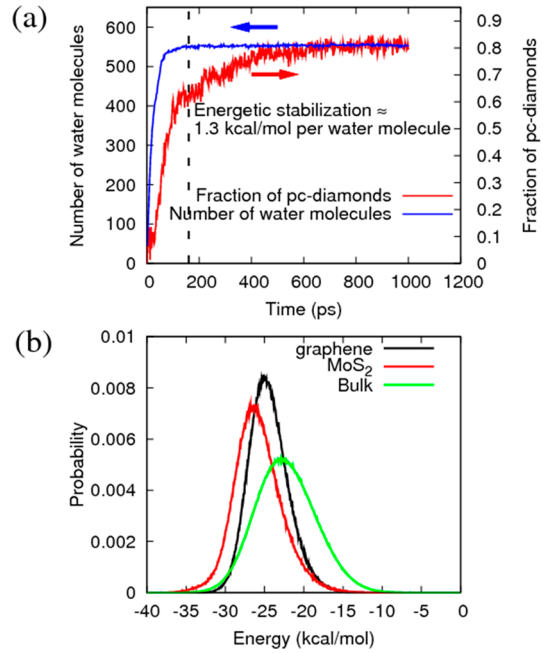

Figure 4. (a) Number of water molecules inserted between MoS_2 sheets (d = 6 Å) and the fraction of water molecules involved in the *pcd* cofiguration as a function of time during equilibration. The vertical line in panel a is positioned at t = 160 ps. (b) Probability distribution of the binding energy of the confined and bulk water molecules.

rapidly fill the space between MoS_2 layers within about 160 ps to obtain the final saturated equilibrium density, but at this stage only about 60% of water molecules are in the *pcd* configuration. It takes an additional 460 ps to reach the 85% *pcd* configuration. The change in total potential energy during the latter period (160 ps < t < 600 ps) reflects the energetic stabilization coming from the configurational rearrangement of water toward the *pcd* array. In other words, the *pcd* formation energy from a random and amorphous state can be estimated by the amount of potential energy lowering by every rearrangement of a confined water molecule into the *pcd* configuration, which results in ∼1.3 kcal/mol, or ∼2.1 k_BT at room temperature, per water molecule.

These planar ordered *pcd* configurations are also persistent in the multilayered water structures. In comparison to the single layer case at d = 6 Å (0.6 ns), the *pcd* formation takes a longer time for d = 8, 11, and 13 Å (as shown in Figure S7, it takes about 4.5 ns to reach 70−90% *pcd*). Nonetheless, it is clear that the *pcd* water ordering observed for the single-layer spacing does remain prevalent in the double, triple, and quadruple structures as well. For graphene, the *pcd* ratio (82%) at d = 6 Å is similar to the case of MoS_2, but for d = 8, 11, and 13 Å without high pressures, the *pcd* configuration is not obtained because of significant interlayer H-bonds.

The binding energy distribution of water molecules confined in between the MoS_2 sheets was analyzed for d = 6 Å and compared with those of the bulk water and graphene. As shown in Figure 4B (and Table 1), the water binding energies between MoS_2 layers are larger (more stable) than the bulk water by 3.5 kcal/mol on average and more sharply distributed due to an ice-like structure of 2D water. In the graphene confinement, the 2D binding is also preferred to the bulk by 2.1 kcal/mol, but it is slightly less stable than in MoS_2. We note in passing that the single-file water molecules inside an ultranarrow carbon nanotube can have a binding energy distribution that is on average more unfavorable compared with bulk water, albeit an entropic gain drives to the 1D confinement eventually.[3]

To understand the origin of the favorable binding energy of the 2D water in the MoS_2 confinement compared with the bulk counterpart, we decomposed the binding energy into the electrostatic and van der Waals interactions in between water molecules and between water and MoS_2 (Table 1). The largest contribution to the favorable binding energy observed in Figure 4B originates from the favorable electrostatic (i.e., H-bond) interaction among water molecules under the 2D confinement. The electrostatic interaction between water and Mo atoms of MoS_2 is largely screened by that between water and S atoms of

DOI: 10.1021/acs.jpcc.7b05153
J. Phys. Chem. C 2017, 121, 16021−16028

Table 1. Average Interaction Energies (kcal/mol) for a Water Molecule Confined between the Two MoS_2 Layers for d = 6 Å[a]

	electrostatic	van der Waals (repulsion + dispersion)	total
water−MoS_2	−0.1	−5.1	−5.2
water−water (MoS_2)	−30.1	9.5	−20.6
total (MoS_2)	−30.2	4.4	−25.8
water−graphene	0.0	−3.8	−3.8
water−water (graphene)	−26.0	5.4	−20.6
total (graphene)	−26.0	1.6	−24.4
bulk water	−26.6	4.3	−22.3

[a]The corresponding values for a water molecule confined between graphene layers and those of bulk water (SPC/E) are listed also for comparison.

Table 2. Areal Density (Å^{-2}) of Water between MoS_2 with Normal and Modified Force Fields[a]

spacing (Å)	MoS_2	MoS_2 (0.5ϵ)	MoS_2 (1.5ϵ)	MoS_2 (q = 0)	graphene
6	0.14 (85%)	0.14 (74%)	0.14 (67%)	0.13 (81%)	0.13 (70%)
8	0.27 (82%)	0.27 (82%)	0.26 (19%)	0.15	0.14
11	0.40 (80%)	0.40 (83%)	0.41 (88%)	0.28	0.28
13	0.52 (76%)	0.53 (82%)	0.53 (74%)	0.35	0.35

[a]"q = 0" denotes the case with setting the charges of Mo and S as zero, and "1.5ϵ" and "0.5ϵ" denote the cases with the Lennard-Jones parameter ϵ adjusted by 1.5 and 0.5 times, respectively. The percentage of water molecules in the *pcd* configuration is given in the parentheses if the planar layered structure is formed. Results for the graphene confinements are also shown for comparison.

MoS_2 such that the electrostatic interaction between water and MoS_2 is sharply distributed near zero. Similarly, the van der Waals interaction among water molecules under the MoS_2 confinement is unfavorable by 9.5 kcal/mol on average (due to a tight water−water H-bond distance described below and associated Pauli repulsion), although partly compensated by the favorable van der Waals interaction between water and MoS_2 to yield eventually a mild, net van der Waals contribution to the water binding energy of 4.4 kcal/mol. This van der Waals contribution to the MoS_2-confined 2D water is nearly identical to that of the water−water van der Waals interaction in the SPC/E bulk water model (4.3 kcal/mol). The binding energy of the confined water in graphene is slightly smaller than that in MoS_2, mostly due to the weaker water−water H-bond (electrostatic) contributions which are rather similar to the bulk water.

The increased water−water electrostatic stabilization and van der Waals repulsion are attributable to the decrease of the average distance between neighboring water molecules when confined between MoS_2 sheets. Thus, the first peak of the O−O radial distribution function (Figure S9C) is shifted closer by 0.05 Å with a pronounced enhancement in the peak height compared with the bulk water. The decrease in the average intermolecular distance is also seen in the two-dimensional plot of the potential of mean force of the H-bond as a function of O···H distance and O−H···O angle (Figure S9A). It shows clearly that the attractive well of the H-bond is much narrower and more focused for the confined water than for the bulk water.

As mentioned above, the key result from the MD is that the monolayer structure of 2D water confined in graphene is quite similar to that for MoS_2, even though graphene is flat and MoS_2 is ratchet-profiled atomically. Nonetheless, the multilayer water structures exhibit major differences in the 2D water structure for MoS_2 and graphene confinements, that is, planar multilayer configurations are obtained in MoS_2 nearly spontaneously.

To understand whether the difference between graphene and MoS_2 confined water structures is due to the presence of charges in MoS_2 or the nonplanar morphology, we performed four sets of simulations. In the first two cases, we assessed the sensitivity of the structural results on the force field used. Here we increased and decreased by 50% the depth of the potential well, ε, of the Lennard-Jones potential $V(r) = 4\epsilon[(\sigma/r)^{12} - (\sigma/r)^6]$ for the interaction between water and MoS_2. In the third case, we turned off the charges of Mo and S atoms of MoS_2 sheets, making them zero so that there is no electrostatic interaction between water and MoS_2, as in graphene, but the ratchet-profiled morphology remains. In the fourth case, we performed the simulations using the infinite graphene slabs at d = 6, 8, 11, and 13 Å, but used the same density of water obtained from the MoS_2 simulations.

For the first two cases of increasing and decreasing ε, we observed no noticeable change in the density or the number of water molecules confined between MoS_2 sheets as can be seen in Tables 2, but just the fraction of water molecules in the *pcd* configuration was reduced from 85% to 67% when increasing ε and to 74% when decreasing ε, showing that the van der Waals interaction has a non-negligible influence on the formation of the ordered *pcd* structure. The planarity of the water layer with increased or decreased ε was similar to the case with the original ε (See Figures S10 and S11). We also used the van der Waals parameters between water and MoS_2 from Liang et al.,[39,40] obtaining 77% for the fraction of water in the *pcd* structure at 6 Å spacing.

For the third case with charges of MoS_2 off, we find that water has great difficulty to enter the sandwiched space between MoS_2 at d = 6 Å. It took about 25 ns to reach an equilibrium water density inside the MoS_2 regions, and the density of water between MoS_2 also decreased about 9% compared to the case with charges on. The fraction of water molecules in the *pcd* structure was 81% when averaged over 4 ns after 25 ns equilibration, not much different from 85% with charges on. This means that the formation of the pc-diamonds structure is rather independent of the electrostatic interaction between water and MoS_2 in the single layer case of 6 Å spacing, which is consistent with the observation in Figure S8 that the distribution of water−MoS_2 electrostatic interaction is centered near zero by the cancellation of the interaction with Mo atoms and that with S atoms.

DOI: 10.1021/acs.jpcc.7b05153
J. Phys. Chem. C 2017, 121, 16021−16028

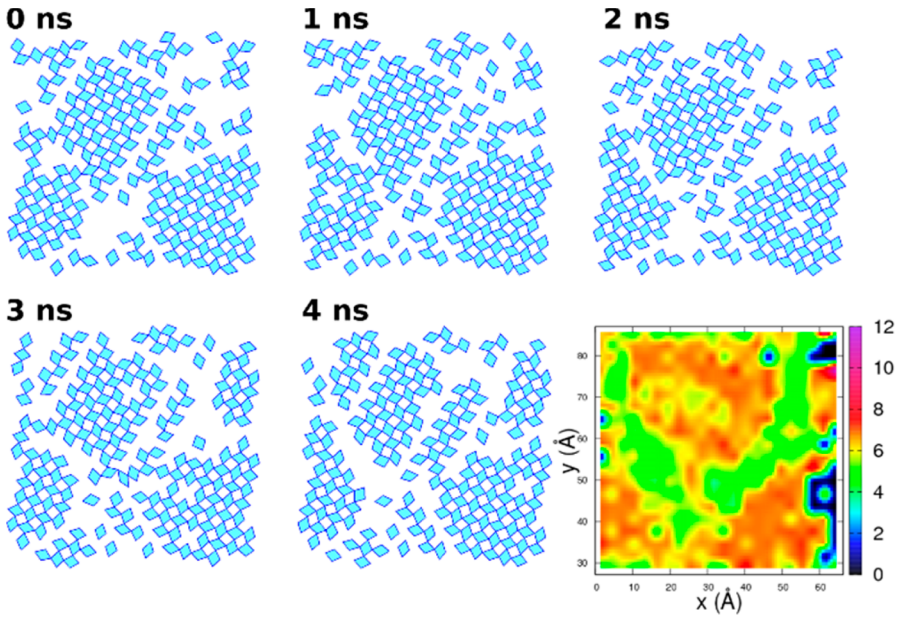

Figure 5. Configuration of the *pcd* structure from the MD snapshots at five different time from 0 to 4 ns for the water molecules between MoS_2 with d = 6 Å spacing. The vertices of the diamonds correspond to the position of oxygen atoms involved in the configuration of the *pcd* structure. In the lower right is the 2D plot of H-bond lifetimes (ps) as a function of position calculated using a 3 × 3 Å grid.

However, we find that the framework charges have significant effects for the multilayered water structures at d = 8, 11, and 13 Å. Noticeably, with the charges of MoS_2 off, the density of confined water molecules for d = 8, 11, and 13 Å is significantly reduced by 30−45% (Table 2) and the previously observed clearly separated water layers do not form with significant interlayer H-bonding interactions, as evident in the density profiles of water molecules in Figure S12. Thus, although the electrostatic interaction between water and MoS_2 was not crucial in the formation of the *pcd* structure for the monolayer case, it is essential for multilayer cases to form ordered flat *pcd* structure, perhaps by allowing a required density for the multilayer *pcd* formation.

To test the density dependent multilayered 2D water formation hypothesis, we performed the MD simulations for water between graphene sheets with the same areal density of water obtained from the equilibrium MoS_2 simulations (densities used in Figures 2 and 3). Interestingly, even for graphene confinements, we now observe well-separated single, double, triple and quadruple layered water structures as shown in Figure S13, and the fraction of water molecules in the *pcd* structure was also 82%, 87%, 90%, and 82% for d = 6, 8, 11, and 13 Å, respectively. These results indicate clearly that, as long as the density is properly tuned, the 2D water can have multilayer planar perpendicularly crossing diamonds structures even in graphene at 1 atm.

The fact that the areal density as well as the fraction of the *pcd* configurations for MoS_2 with q = 0 (charges off) cases are almost the same as those of graphene (Table 2) suggests that the ratchet-profiled (MoS_2) or flat (graphene) morphology is not a dominant factor in determining the structure of 2D water. The detailed morphology (flat vs ratchet-profiled) of confinements in graphene or MoS_2 thus seems to play a minor role in determining the structure of 2D water as long as the density is determined via the polarity of the surface.

As shown in Figure S14B, the average number of H-bonds per water molecule shows a local maximum (3.70−3.76) when the planar water layers are formed at d = 6, 8, 11, and 13 Å. To investigate the dynamic nature of H-bonds we calculated the H-bond correlation function[41,42] defined as $C_{HB}(t) = \langle h(0)h(t)\rangle / \langle h\rangle$ where $h(t)$ = 1 when a tagged water molecule at time zero is bonded to the same H-bond partner molecule at time t, and $h(t)$ = 0 otherwise. The $C_{HB}(t)$ shows a fast initial decay within 1 ps and then an extremely slow decay at longer times (Figure S15). When the slowly decaying part is fitted to the exponential function $e^{-t/\tau}$, we obtain τ = 32 ns. The slow decay of $C_{HB}(t)$ represents a situation that when a H-bond between a pair of water molecules is broken, the pair does not diffuse away but reforms a H-bond, so that the configurational change of the confined water is very slow. This slow relaxation time scale of 32 ns of the *pcd* configuration represents ice-like nature of the confined water.

Figure 5 shows the time evolution of the *pcd* structure of water for d = 6 Å. Over 4 ns, the structure of the initially formed *pcd* moieties is well conserved with only minor local fluctuations. The 2D plot of the average H-bond lifetime in 3 × 3 Å grids (Figure 5) shows that the regions of longer H-bond lifetimes match very well the regions of higher population for the *pcd* array. This result shows that the H-bond breaking and reforming is more frequent at the boundaries of the ordered *pcd* regions.

CONCLUSIONS

In summary, we used molecular dynamics simulations to predict the multilayered planar H-bonded structures of water confined in between MoS_2 sheets at ambient conditions, in contrast to graphene confinement. These 2D H-bonds show a pattern consisting of both square and rhomboidal local moieties with a perpendicularly crossing (*pcd*) configuration forming an isogonal tiling. More than 80% of confined water molecules participate in the ordered *pcd* configuration, both in monolayer and multilayer cases, with an extremely long H-bond lifetime comparable to that of ice. Controlled simulations with modified force field suggest that the polar nature (atomic charges) of 2D

DOI: 10.1021/acs.jpcc.7b05153
J. Phys. Chem. C 2017, 121, 16021−16028

MoS_2 allows a higher density of water under confinement than in graphene, leading to a stable, multilayered planar water structure, whereas a detailed morphology of the confinement (ratchet-profiled or flat) does not play a primary role. Our findings of the water H-bond configuration in the 2D confinement provided by MoS_2 suggest interesting differences in the nanofluidic transport of water in MoS_2 channels and lamellar membranes.[38] This may provide a new design tool for applications to energy and environment.

■ ASSOCIATED CONTENT

Supporting Information

The Supporting Information is available free of charge on the ACS Publications website at DOI: 10.1021/acs.jpcc.7b05153.

Details of MD simulations and analyses for force field validation, density profiles, water orientation distributions, H-bond distribution, and time-correlation function (PDF)

■ AUTHOR INFORMATION

Corresponding Author

*(Y.J.) E-mail: ysjn@kaist.ac.kr.

ORCID

Tod A. Pascal: 0000-0003-2096-1143
William A. Goddard: 0000-0003-0097-5716
Hyung Gyu Park: 0000-0001-8121-2344
Yousung Jung: 0000-0003-2615-8394

Notes

The authors declare no competing financial interest.

■ ACKNOWLEDGMENTS

We acknowledge the financial support of the Climate Change Research Hub Project of the KAIST EEWS Research Center (EEWS-2017-N11170056). H.G.P. appreciates supports from the Swiss National Science Foundation (NRP 70 "Energy Turnaround" 407040_153978) and CTI Energy Program (SCCER Heat & Electricity Storage) of Switzerland, and is also grateful to Korea Institute of Energy Technology Evaluation and Planning and the Ministry of Trade, Industry, & Energy of the Republic of Korea (20168510011420).

■ REFERENCES

(1) Bocquet, L.; Charlaix, E. *Chem. Soc. Rev.* **2010**, *39*, 1073−1095.
(2) Park, H. G.; Jung, Y. Carbon Nanofluidics of Rapid Water Transport for Energy Applications. *Chem. Soc. Rev.* **2014**, *43*, 565−576.
(3) Hummer, G.; Rasaiah, J. C.; Noworyta, J. P. Water Conduction through the Hydrophobic Channel of a Carbon Nanotube. *Nature* **2001**, *414*, 188−190.
(4) Majumder, M.; Chopra, N.; Andrews, R.; Hinds, B. J. Nanoscale Hydrodynamics: Enhanced Flow in Carbon Nanotubes. *Nature* **2005**, *438*, 44−44.
(5) Holt, J. K.; Park, H. G.; Wang, Y.; Stadermann, M.; Artyukhin, A. B.; Grigoropoulos, C. P.; Noy, A.; Bakajin, O. Fast Mass Transport through Sub-2-Nanometer Carbon Nanotubes. *Science* **2006**, *312*, 1034−1037.
(6) Whitby, M.; Cagnon, L.; Thanou, M.; Quirke, N. Enhanced Fluid Flow through Nanoscale Carbon Pipes. *Nano Lett.* **2008**, *8*, 2632−2637.
(7) Qin, X.; Yuan, Q.; Zhao, Y.; Xie, S.; Liu, Z. Measurement of the Rate of Water Translocation through Carbon Nanotubes. *Nano Lett.* **2011**, *11*, 2173−2177.
(8) Koga, K.; Tanaka, H.; Zeng, X. C. First-Order Transition in Confined Water between High-Density Liquid and Low-Density Amorphous Phases. *Nature* **2000**, *408*, 564−567.
(9) Giovambattista, N.; Rossky, P. J.; Debenedetti, P. G. Phase Transitions Induced by Nanoconfinement in Liquid Water. *Phys. Rev. Lett.* **2009**, *102*, 050603.
(10) Koga, K.; Tanaka, H. Phase Diagram of Water between Hydrophobic Surfaces. *J. Chem. Phys.* **2005**, *122*, 104711.
(11) Kumar, P.; Buldyrev, S. V.; Starr, F. W.; Giovambattista, N.; Stanley, H. E. Thermodynamics, Structure, and Dynamics of Water Confined between Hydrophobic Plates. *Phys. Rev. E* **2005**, *72*, 051503.
(12) Koga, K.; Gao, G. T.; Tanaka, H.; Zeng, X. C. Formation of Ordered Ice Nanotubes inside Carbon Nanotubes. *Nature* **2001**, *412*, 802−805.
(13) Takaiwa, D.; Hatano, I.; Koga, K.; Tanaka, H. Phase Diagram of Water in Carbon Nanotubes. *Proc. Natl. Acad. Sci. U. S. A.* **2008**, *105*, 39−43.
(14) Pascal, T. A.; Goddard, W. A.; Jung, Y. Entropy and the Driving Force for the Filling of Carbon Nanotubes with Water. *Proc. Natl. Acad. Sci. U. S. A.* **2011**, *108*, 11794−11798.
(15) Waghe, A.; Rasaiah, J. C.; Hummer, G. Entropy of Single-File Water in (6,6) Carbon Nanotubes. *J. Chem. Phys.* **2012**, *137*, 044709.
(16) Zhao, W.-H.; Wang, L.; Bai, J.; Yuan, L.-F.; Yang, J.; Zeng, X. C. Highly Confined Water: Two-Dimensional Ice, Amorphous Ice, and Clathrate Hydrates. *Acc. Chem. Res.* **2014**, *47*, 2505−2513.
(17) Zhao, W.-H.; Bai, J.; Yuan, L.-F.; Yang, J.; Zeng, X. C. Ferroelectric Hexagonal and Rhombic Monolayer Ice Phases. *Chem. Sci.* **2014**, *5*, 1757−1764.
(18) Zangi, R.; Mark, A. E. Monolayer Ice. *Phys. Rev. Lett.* **2003**, *91*, 025502.
(19) Han, S.; Choi, M. Y.; Kumar, P.; Stanley, H. E. Phase Transitions in Confined Water Nanofilms. *Nat. Phys.* **2010**, *6*, 685−689.
(20) Bai, J.; Zeng, X. C. Polymorphism and Polyamorphism in Bilayer Water Confined to Slit Nanopore under High Pressure. *Proc. Natl. Acad. Sci. U. S. A.* **2012**, *109*, 21240−21245.
(21) Chen, J.; Schusteritsch, G.; Pickard, C. J.; Salzmann, C. G.; Michaelides, A. Two Dimensional Ice from First Principles: Structures and Phase Transitions. *Phys. Rev. Lett.* **2016**, *116*, 025501.
(22) Zangi, R. Water Confined to a Slab Geometry: A Review of Recent Computer Simulation Studies. *J. Phys.: Condens. Matter* **2004**, *16*, S5371.
(23) Zhu, Y.; Wang, F.; Bai, J.; Zeng, X. C.; Wu, H. Formation of Trilayer Ices in Graphene Nanocapillaries under High Lateral Pressure. *J. Phys. Chem. C* **2016**, *120*, 8109−8115.
(24) Bai, J.; Angell, C. A.; Zeng, X. C. Guest-Free Monolayer Clathrate and Its Coexistence with Two-Dimensional High-Density Ice. *Proc. Natl. Acad. Sci. U. S. A.* **2010**, *107*, 5718−5722.
(25) Kaneko, T.; Bai, J.; Yasuoka, K.; Mitsutake, A.; Zeng, X. C. New Computational Approach to Determine Liquid−Solid Phase Equilibria of Water Confined to Slit Nanopores. *J. Chem. Theory Comput.* **2013**, *9*, 3299−3310.
(26) Zangi, R.; Mark, A. E. Bilayer Ice and Alternate Liquid Phases of Confined Water. *J. Chem. Phys.* **2003**, *119*, 1694−1700.
(27) Zhu, Y.; Wang, F.; Bai, J.; Zeng, X. C.; Wu, H. Compression Limit of Two-Dimensional Water Constrained in Graphene Nanocapillaries. *ACS Nano* **2015**, *9*, 12197−12204.
(28) Zhu, Y.; Wang, F.; Bai, J.; Zeng, X. C.; Wu, H. AB-Stacked Square-Like Bilayer Ice in Graphene Nanocapillaries. *Phys. Chem. Chem. Phys.* **2016**, *18*, 22039−22046.
(29) Sobrino Fernandez Mario, M.; Neek-Amal, M.; Peeters, F. M. AA-Stacked Bilayer Square Ice between Graphene Layers. *Phys. Rev. B: Condens. Matter Mater. Phys.* **2015**, *92*, 245428.
(30) Algara-Siller, G.; Lehtinen, O.; Wang, F. C.; Nair, R. R.; Kaiser, U.; Wu, H. A.; Geim, A. K.; Grigorieva, I. V. Square Ice in Graphene Nanocapillaries. *Nature* **2015**, *519*, 443−445.
(31) Zhou, W.; et al. The Observation of Square Ice in Graphene Questioned. *Nature* **2015**, *528*, E1−E2.

DOI: 10.1021/acs.jpcc.7b05153
J. Phys. Chem. C 2017, 121, 16021−16028

(32) Berendsen, H. J. C.; Grigera, J. R.; Straatsma, T. P. The Missing Term in Effective Pair Potentials. *J. Phys. Chem.* **1987**, *91*, 6269−6271.
(33) Perdew, J. P.; Burke, K.; Ernzerhof, M. Generalized Gradient Approximation Made Simple. *Phys. Rev. Lett.* **1996**, *77*, 3865−3868.
(34) Moellmann, J.; Grimme, S. Importance of London Dispersion Effects for the Packing of Molecular Crystals: A Case Study for Intramolecular Stacking in a Bis-Thiophene Derivative. *Phys. Chem. Chem. Phys.* **2010**, *12*, 8500−8504.
(35) Hockney, R. W.; Eastwood, J. W. *Computer Simulation Using Particles*; CRC Press: 1988.
(36) Plimpton, S. Fast Parallel Algorithms for Short-Range Molecular Dynamics. *J. Comput. Phys.* **1995**, *117*, 1−19.
(37) Luzar, A.; Chandler, D. Hydrogen-Bond Kinetics in Liquid Water. *Nature* **1996**, *379*, 55−57.
(38) Deng, M.; Kwac, K.; Li, M.; Jung, Y.; Park, H. G. Stability, Molecular Sieving, and Ion Diffusion Selectivity of a Lamellar Membrane from Two-Dimensional Molybdenum Disulfide. *Nano Lett.* **2017**, *17*, 2342.
(39) Heiranian, M.; Farimani, A. B.; Aluru, N. R. Water Desalination with a Single-Layer Mos2 Nanopore. *Nat. Commun.* **2015**, *6*, 8616.
(40) Liang, T.; Phillpot, S. R.; Sinnott, S. B. Parametrization of a Reactive Many-Body Potential for Mos2 Systems. *Phys. Rev. B: Condens. Matter Mater. Phys.* **2009**, *79*, 245110.
(41) Chandra, A. Effects of Ion Atmosphere on Hydrogen-Bond Dynamics in Aqueous Electrolyte Solutions. *Phys. Rev. Lett.* **2000**, *85*, 768−771.
(42) Winarto; Takaiwa, D.; Yamamoto, E.; Yasuoka, K. Structures of Water Molecules in Carbon Nanotubes under Electric Fields. *J. Chem. Phys.* **2015**, *142*, 124701.

DOI: 10.1021/acs.jpcc.7b05153
J. Phys. Chem. C 2017, 121, 16021−16028